JOURNAL OF COMPUTATIONAL PHYSICS 71, 65–99 (1987)

Symmetry of the Flow around a Circular Cylinder

V. A. PATEL

Department of Mathematics, Humboldt State University, Arcata, California 95521

Received Auguest 21, 1985; revised October 1, 1986

The symmetry of the two-dimensional, viscous, and incompressible flow past a circular cylinder is studied by disturbing impulsively the steady flow at Reynolds number 10, 20, 40, and 100. The propagation of this disturmbance is studied by dividing the stream and vorticity functions into steady and perturbed stream and vorticity functions. The steady stream and vorticity functions are expanded in the finite Fourier sine series. The steady semianalytical solutions are obtained for the symmetrical flow as a limit of the time-dependent equations. The perturbed stream and vorticity functions are expanded in the finite Fourier sine and cosine series and then along with the steady stream and vorticity functions expansions substituted in the Navier–Stokes equations. This leads to a system of coupled parabolic partial differential equations in the coefficient functions of Fourier series which is solved numerically. This system is solved with the initial condition which corresponds to the applied impulsive velocity to the surface of the cylinder in the perpendicular direction of the flow. Asymmetric vortices are observed for the Reynolds number (Re) 40 and a slight oscillation of the trail of almost symmetrical wakes is seen for the Reynolds numbers 20 up to $t = 100$. The symmetrical standing vortices in the strictest sense are not observed for $\mathrm{Re} = 10$ even up to $t = 100$. Vortex shedding is observed for $\mathrm{Re} = 100$. For Reynolds number 10, the disturbance is applied continuously up to $t = 1$, and asymmetric vortices exist up to $t = 100$. The symmetry of the flow depends on the disturbance level in the flow even at Reynolds number 10.

1. INTRODUCTION

The problem of finding the flow past a circular cylinder is a classical one with an extensive literature; however, many questions remain unanswered. Coutanceau and Bouard [3] and Gerrard [8] determined that at $\mathrm{Re} = 34$, the standing vortices become asymmetric, while Taneda [17] found that the wake begins to oscillate at $\mathrm{Re} = 30$, where Reynolds number is defined by $\mathrm{Re} = 2aU/\nu$, where a is the radius of the cylinder, U is the free stream velocity, and ν is the kinematic viscosity. The measurements of the Strouhal number by Gerrard [8] in the Reynolds number range up to 350 are lower than those of Rosko [15, 16] and Tritton [19], and so Gerrard suggested that this quantity may depend upon the disturbance level in the flow. Taneda [18] has shown that close behind a cylinder, the wake can be made to oscillate by oscillating the cylinder for Re barely above unity. The following question can be raised: Does the initial disturbance play an important role for the flow to be aymmetric around a circular cylinder? If the answer is yes, then is it possible to have an asymmetrical flow at lower Reynolds numbers? In order to

0021-9991/87 $3.00

answer this question theoretically, the stability of the wake behind the cylinder is to be studied. The basic idea is to disturb the steady flow and then observe whether the disturbance dies away, persists as a disturbance of similar magnitude or grows so much that the steady flow becomes a different flow (see, e.g., Drazin and Reid [6]).

Since we do not have as yet the exact steady solution for the flow past a circular cylinder, semianalytic solutions for the steady flow are first obtained as a limit of the time-dependent equations for various Reynolds numbers by using the finite series truncation method. Desai [5] obtained solutions by expanding the stream and vorticity functions in finite Fourier series for the steady flow of a viscous incompressible fluid past a circular cylinder for $\mathrm{Re} = 1$–40. Underwood [20], Dennis and Chang [4], Niewstadt and Keller [11], and Jafroudi and Yang [9] obtained the semianalytic solutions for the steady flows. Collins and Dennis [2] and Patel [12] obtained the semianalytic solutions for the impulsively started symmetric flows. Using the finite series truncation method, Patel [13, 14] obtained Kármán vortex street behind a circular cylinder for $\mathrm{Re} = 100$, 200, and 500, and semianalytic solutions for the impulsively started elliptic cylinder at various angles of attack.

The steady semianalytic solution is disturbed, and the propagation of the disturbance in space and time is observed in much the same way as in the laboratory experiment. The development of the disturbance is determined by expanding the disturbed stream and vorticity functions in the Fourier sine and cosine series and then substituting along with the steady stream and vorticity expansions in the Navier–Stokes equations for two-dimensional, viscous, and incompressible flows. This leads to a system of coupled parabolic partial differential equations in terms of the coefficient functions of Fourier series. This mathematical formulation is given in Section 2. In Section 3, we discuss the numerical solution technique of this coupled system. The disturbances and solutions are discussed in Section 4. This investigation is restricted by the assumption of two dimensionality and, therefore, valid as long as two-dimensional effects play the dominant role in the physical flow.

2. Basic Equations and Analysis

Consider a steady laminar flow of a viscous incompressible fluid around a circular cylinder of radius a. At time $t = 0$, the flow is disturbed. The equations which are assumed to govern the subsequent motions are the Navier–Stokes equations and the equation of continuity, which are coupled and to be solved subject to the boundary conditions of no slip on the surface of the cylinder and irrotational flow at infinity.

The governing equation of motion, nondimensionalised with reference to the free stream speed and the cylinder radius, can be written as

$$\frac{\partial \zeta}{\partial t} + \frac{1}{r}\left(\frac{\partial \Psi}{\partial \theta}\frac{\partial \zeta}{\partial r} - \frac{\partial \Psi}{\partial r}\frac{\partial \zeta}{\partial \theta}\right) = \frac{2}{\mathrm{Re}}\nabla^2 \zeta, \tag{2.1}$$

where

$$\nabla^2 = \frac{\partial^2}{\partial r^2} + \frac{1}{r}\frac{\partial}{\partial r} + \frac{1}{r^2}\frac{\partial^2}{\partial \theta^2}. \tag{2.2}$$

The stream function Ψ, the vorticity ζ and the velocity components u and v in the r and θ directions are connected by the relations

$$\zeta = -\nabla^2 \Psi, \tag{2.3}$$

$$u = \frac{1}{r}\frac{\partial \Psi}{\partial \theta} \qquad \text{and} \qquad v = -\frac{\partial \Psi}{\partial r}. \tag{2.4}$$

The boundary conditions that are imposed upon the body surface are the usual impermeability and no slip condition for all time. As the distance from the cylinder becomes very large, it is assumed that the flow will approach more and more that of an irrotational flow. These boundary conditions can be written as
For $t \geqslant 0$,

$$\Psi = \frac{\partial \Psi}{\partial r} = 0 \qquad \text{at} \quad r = 1, \tag{2.5}$$

and

$$\Psi = -\left(r - \frac{1}{r}\right)\sin\theta \qquad \text{and, therefore, from (2.3)} \qquad \zeta = 0 \quad \text{as} \quad r \to \infty. \tag{2.6}$$

It is convenient to work with the deviation ψ from the irrotational flow instead of Ψ so let us write

$$\Psi(r, \theta) = \psi(r, \theta, t) - \left(r - \frac{1}{r}\right)\sin\theta. \tag{2.7}$$

The logarithmic transformation $\xi = \ln r$ of the radial coordinate is desirable since the cells of the log-polar grid are smaller near the cylinder where the largest gradients occur in the flow. Equations (2.1), (2.2), and (2.3), by using (2.7) and $\xi = \ln r$, reduce to

$$\frac{\partial \zeta}{\partial t} + e^{-2\xi}\left[\frac{\partial \psi}{\partial \theta}\frac{\partial \zeta}{\partial \xi} - \frac{\partial \psi}{\partial \xi}\frac{\partial \zeta}{\partial \theta} + (e^{\xi} + e^{-\xi})\sin\theta\frac{\partial \zeta}{\partial \theta} - (e^{\xi} - e^{-\xi})\cos\theta\frac{\partial \zeta}{\partial \xi}\right] = \frac{2}{\mathrm{Re}}\nabla^2\zeta, \tag{2.8}$$

where $\nabla^2 = (\partial^2/\partial\xi^2) + (\partial^2/\partial\theta^2)$ and

$$\zeta = -e^{-2\xi}\nabla^2\psi. \tag{2.9}$$

Substitution of (2.7) and $\xi = \ln r$ reduces (2.5) and (2.6) to, for $t \geqslant 0$,

$$\psi = 0 \qquad \text{and} \qquad \frac{\partial \psi}{\partial \xi} = 2 \sin \theta \quad \text{at} \quad \xi = 0 \tag{2.10}$$

and

$$\psi = \zeta = 0 \quad \text{as} \quad \xi \to \infty. \tag{2.11}$$

Consider a disturbance stream function $\hat{\psi}(\xi, \theta, t)$ to be superimposed on the steady laminar flow $\bar{\psi}(\xi, \theta)$. This leads to

$$\psi(\xi, \theta, t) = \bar{\psi}(\xi, \theta) + \hat{\psi}(\xi, \theta, t) \tag{2.12}$$

and

$$\zeta(\xi, \theta, t) = \bar{\zeta}(\xi, \theta) + \hat{\zeta}(\xi, \theta, t), \tag{2.13}$$

where $\bar{\psi}$ and $\bar{\zeta}$ satisfy (2.8), (2.9), (2.10), and (2.11). In other words,

$$\frac{\partial \bar{\psi}}{\partial \theta}\frac{\partial \bar{\psi}}{\partial \xi} - \frac{\partial \bar{\psi}}{\partial \xi}\frac{\partial \bar{\zeta}}{\partial \theta} + (e^{\xi} + e^{-\xi}) \sin \theta \frac{\partial \bar{\zeta}}{\partial \theta} - (e^{\xi} - e^{-\xi}) \cos \theta \frac{\partial \bar{\zeta}}{\partial \xi} = \frac{2e^{2\xi}}{\mathrm{Re}} \nabla^2 \bar{\zeta}, \tag{2.14}$$

where

$$\bar{\zeta} = -e^{-2\xi} \nabla^2 \bar{\psi}, \tag{2.15}$$

$$\bar{\psi} = 0 \qquad \text{and} \qquad \frac{\partial \bar{\psi}}{\partial \xi} = 2 \sin \theta \quad \text{at} \quad \xi = 0 \tag{2.16}$$

and

$$\bar{\psi} = \bar{\zeta} = 0 \qquad \text{as} \quad \zeta \to \infty. \tag{2.17}$$

Substitution of (2.12) and (2.13) in (2.8), (2.9), (2.10), and (2.11) along with (2.14), (2.15), (2.16), and (2.17) leads to

$$\frac{\partial \hat{\zeta}}{\partial t} + e^{-2\xi}\left[\frac{\partial \bar{\psi}}{\partial \theta}\frac{\partial \hat{\zeta}}{\partial \xi} - \frac{\partial \bar{\psi}}{\partial \xi}\frac{\partial \hat{\zeta}}{\partial \theta} + \frac{\partial \hat{\psi}}{\partial \theta}\frac{\partial \bar{\zeta}}{\partial \xi} - \frac{\partial \hat{\psi}}{\partial \xi}\frac{\partial \bar{\zeta}}{\partial \theta} + \frac{\partial \hat{\psi}}{\partial \theta}\frac{\partial \hat{\zeta}}{\partial \xi} - \frac{\partial \hat{\psi}}{\partial \xi}\frac{\partial \hat{\zeta}}{\partial \theta}\right.$$
$$\left. + (e^{\xi} + e^{-\xi}) \sin \theta \frac{\partial \hat{\zeta}}{\partial \theta} - (e^{\xi} - e^{-\xi}) \cos \theta \frac{\partial \hat{\zeta}}{\partial \xi}\right] = \frac{2}{\mathrm{Re}} \nabla^2 \hat{\zeta}, \tag{2.18}$$

where

$$\hat{\zeta} = -e^{-2\xi} \nabla^2 \hat{\psi}. \tag{2.19}$$

For $t \geqslant 0$,

$$\hat{\psi} = \frac{\partial \hat{\psi}}{\partial \xi} = 0 \qquad \text{at} \quad \xi = 0 \tag{2.20}$$

and

$$\hat{\psi} = \hat{\zeta} = 0 \qquad \text{as} \quad \xi \to \infty. \tag{2.21}$$

Since the steady flow is assumed to be symmetrical, the stream function $\bar{\psi}(\xi, \theta)$ can be expanded in a Fourier sine series

$$\bar{\psi}(\xi, \theta) = \sum_{n=1}^{\infty} f_n(\xi) \sin n\theta. \tag{2.22}$$

Use of (2.22) in (2.15) leads to

$$\bar{\zeta}(\xi, \theta) = -\sum_{n=1}^{\infty} F_n(\xi) \sin n\theta, \tag{2.23}$$

where

$$F_n(\xi) = e^{-2\xi}\left(\frac{d^2 f_n}{d\xi^2} - n^2 f_n\right). \tag{2.24}$$

Substitution of (2.22) and (2.23) in (2.16) and (2.17) leads to

$$f_n(0) = 0 \qquad \text{for} \quad n = 1, 2, \ldots,$$

$$\frac{\partial f_1}{\partial \xi}(0) = 2 \qquad \text{and} \qquad \frac{\partial f_m}{\partial \xi}(0) = 0 \quad \text{for} \quad m = 2, 3, \ldots \tag{2.25}$$

and

$$f_n(\xi_\infty) = F_n(\xi_\infty) = 0 \qquad \text{for} \quad n = 1, 2, \ldots. \tag{2.26}$$

Let us assume that $\hat{\psi}(\xi, \theta, t)$ is a reasonably well-behaved function throughout the domain, so that it can be represented in a Fourier series

$$\hat{\psi}(\xi, \theta, t) = a_0(\xi, t) + \sum_{n=1}^{\infty} (a_n(\xi, t) \cos n\theta + b_n(\xi, t) \sin n\theta), \tag{2.27}$$

where a_0, a_n, and b_n are the functions to be determined.

Using (2.27) in (2.19) yields

$$\hat{\zeta}(\xi, \theta, t) = -A_0(\xi, t) - \sum_{n=1}^{\infty} (A_n(\xi, t) \cos n\theta + B_n(\xi, t) \sin n\theta), \tag{2.28}$$

where $A_0(\xi, t) = e^{-2\xi}(\partial^2 a_0/\partial\xi^2)$, $A_n(\xi, t) = e^{-2\xi}((\partial^2 a_n/\partial\xi^2) - n^2 a_n)$, and

$$B_n(\xi, t) = e^{-2\xi}\left(\frac{\partial^2 b_n}{\partial\xi^2} - n^2 b_n\right). \tag{2.29}$$

Substitution of (2.22), (2.23), (2.27), and (2.28) in (2.18) leads to an equation in which the terms of $\sin n\theta$ and $\cos n\theta$ are linearly independent, so the equation is satisfied only if the coefficients of $\sin n\theta$ and $\cos n\theta$ are identically equal to zero. This leads to

$$\begin{aligned}
&\frac{\partial A_0}{\partial t} - \frac{e^{-2\xi}}{2}\left\{\frac{4}{\mathrm{Re}}\frac{\partial^2 A_0}{\partial\xi^2} + (e^{\xi} - e^{-\xi})\frac{\partial A_1}{\partial\xi} + (e^{\xi} + e^{-\xi})A_1\right. \\
&\quad - \sum_{m=1}^{\infty} m\left[A_m\frac{df_m}{d\xi} - a_m\frac{dF_m}{d\xi} - F_m\frac{\partial a_m}{\partial\xi} + b_m\frac{\partial A_m}{\partial\xi} - a_m\frac{\partial B_m}{\partial\xi}\right. \\
&\quad \left.\left. - B_m\frac{\partial a_m}{\partial\xi} + A_m\frac{\partial b_m}{\partial\xi} + f_m\frac{\partial A_m}{\partial\xi}\right]\right\} = 0, \qquad (2.30)
\end{aligned}$$

$$\begin{aligned}
&\frac{\partial A_1}{\partial t} - \frac{e^{-2\xi}}{2}\left\{\frac{4}{\mathrm{Re}}\left(\frac{\partial^2 A_1}{\partial\xi^2} - A_1\right) + (e^{\xi} - e^{-\xi})\left(2\frac{\partial A_0}{\partial\xi} + \frac{\partial A_2}{\partial\xi}\right)\right. \\
&\quad + 2(e^{\xi} + e^{-\xi})A_2 + \sum_{m=1}^{\infty} m\left[a_m\left(\frac{dF_{m+1}}{d\xi} + \frac{dF_{m-1}}{d\xi} + \frac{\partial B_{m+1}}{\partial\xi} + \frac{\partial B_{m-1}}{\partial\xi}\right)\right. \\
&\quad - A_m\left(\frac{df_{m+1}}{d\xi} + \frac{df_{m-1}}{d\xi} + \frac{\partial b_{m+1}}{\partial\xi} + \frac{\partial b_{m-1}}{\partial\xi}\right) - b_m\left(\frac{\partial A_{m+1}}{\partial\xi} + \frac{\partial A_{m-1}}{\partial\xi}\right) \\
&\quad + B_m\left(\frac{\partial a_{m+1}}{\partial\xi} + \frac{\partial a_{m-1}}{\partial\xi}\right) - f_m\left(\frac{\partial A_{m+1}}{\partial\xi} + \frac{\partial A_{m-1}}{\partial\xi}\right) \\
&\quad \left.\left. + F_m\left(\frac{\partial a_{m+1}}{\partial\xi} + \frac{\partial a_{m-1}}{\partial\xi}\right)\right]\right\} = 0, \qquad (2.31)
\end{aligned}$$

$$\begin{aligned}
&\frac{\partial A_n}{\partial t} - \frac{e^{-2\xi}}{2}\left\{\frac{4}{\mathrm{Re}}\left(\frac{\partial^2 A_n}{\partial\xi^2} - n^2 A_n\right) + (e^{\xi} - e^{-\xi})\left(\frac{\partial A_{n-1}}{\partial\xi} + \frac{\partial A_{n+1}}{\partial\xi}\right)\right. \\
&\quad + (e^{\xi} + e^{-\xi})[(n+1)A_{n+1} - (n-1)A_{n-1}] + \sum_{m=1}^{\infty} m\left[a_m\left(\frac{dF_{m+n}}{d\xi} + \frac{dF_{m-n}}{d\xi}\right.\right. \\
&\quad \left. + \frac{\partial B_{m+n}}{\partial\xi} + \frac{\partial B_{m-n}}{\partial\xi}\right) - A_m\left(\frac{df_{m+n}}{d\xi} + \frac{df_{m-n}}{d\xi} + \frac{\partial b_{m+n}}{\partial\xi} + \frac{\partial b_{m-n}}{\partial\xi}\right) \\
&\quad - b_m\left(\frac{\partial A_{m+n}}{\partial\xi} + \frac{\partial A_{m-n}}{\partial\xi}\right) + B_m\left(\frac{\partial a_{m+n}}{\partial\xi} + \frac{\partial a_{m-n}}{\partial\xi}\right) - f_m\left(\frac{\partial A_{m+n}}{\partial\xi} + \frac{\partial A_{m-n}}{\partial\xi}\right) \\
&\quad \left.\left. + F_m\left(\frac{\partial a_{m+n}}{\partial\xi} + \frac{\partial a_{m-n}}{\partial\xi}\right)\right]\right\} = 0 \qquad \text{for} \quad n = 2, 3, \ldots, \qquad (2.32)
\end{aligned}$$

and

$$\frac{\partial B_n}{\partial t}-\frac{e^{-2\xi}}{2}\left\{\frac{4}{\mathrm{Re}}\left(\frac{\partial^2 B_n}{\partial \xi^2}-n^2 B_n\right)+(e^{\xi}-e^{-\xi})\left(\frac{\partial B_{n-1}}{\partial \xi}+\frac{\partial B_{n+1}}{\partial \xi}\right)\right.$$
$$+(e^{\xi}+e^{-\xi})[(n+1)B_{n+1}-(n-1)B_{n-1}]+\sum_{m=1}^{\infty} m\left[-a_m\left(\frac{\partial A_{m+n}}{\partial \xi}-\frac{\partial A_{m-n}}{\partial \xi}\right)\right.$$
$$+A_m\left(\frac{\partial a_{m+n}}{\partial \xi}-\frac{\partial a_{m-n}}{\partial \xi}\right)-b_m\left(\frac{dF_{m+n}}{d\xi}-\frac{dF_{m-n}}{d\xi}+\frac{\partial B_{m+n}}{\partial \xi}-\frac{\partial B_{m-n}}{\partial \xi}\right)$$
$$+B_m\left(\frac{df_{m+n}}{d\xi}-\frac{df_{m-n}}{d\xi}+\frac{\partial b_{m+n}}{\partial \xi}-\frac{\partial b_{m-n}}{\partial \xi}\right)-f_m\left(\frac{\partial B_{m+n}}{\partial \xi}-\frac{\partial B_{m-n}}{\partial \xi}\right)$$
$$\left.\left.+F_m\left(\frac{\partial b_{m+n}}{\partial \xi}-\frac{\partial b_{m-n}}{\partial \xi}\right)\right]\right\}=0 \qquad \text{for} \quad n=1, 2,..., \tag{2.33}$$

where

$$B_{-n}=-B_n, \qquad A_{-n}=A_n, \qquad F_{-n}=-F_n, \qquad f_{-n}=-f_n,$$
$$a_{-n}=a_n, \qquad b_{-n}=-b_n, \qquad \text{and} \qquad B_0=0. \tag{2.34}$$

Use of (2.27) and (2.28) in (2.20) and (2.21) yields for $t \geqslant 0$,

$$b_n(0, t)=\frac{\partial b_n}{\partial \xi}(0, t)=0 \qquad \text{for} \quad n=1, 2,...,$$
$$a_m(0, t)=\frac{\partial a_m}{\partial \xi}(0, t)=0 \qquad \text{for} \quad m=0, 1,... \tag{2.35}$$

and

$$b_n(\xi_\infty, t)=B_n(\xi_\infty, t)=0 \qquad \text{for} \quad n=1, 2,...,$$
$$a_m(\xi_\infty, t)=A_m(\xi_\infty, t)=0 \qquad \text{for} \quad m=0, 1,.... \tag{2.36}$$

Equations (2.29), (2.30), (2.31), (2.32), (2.33), and (2.34) along with boundary conditions (2.35) and (2.36) form a coupled nonlinear infinite system of partial differential equations to be solved for a_0, a_n, b_n, A_0, A_n, and B_n for given f_n and F_n. Once this system is solved, the flow field is known since the stream and vorticity functions can be reconstructed from the assumed series expansions

$$\psi(\xi, \theta, t)=a_0(\xi, t)+\sum_{n=1}^{\infty}[a_n(\xi, t)\cos n\theta+(f_n(\xi)+b_n(\xi, t))\sin n\theta] \tag{2.37}$$

and

$$\zeta(\xi, \theta, t)=-A_0(\xi, t)-\sum_{n=1}^{\infty}[A_n(\xi, t)\cos n\theta+(F_n(\xi)+B_n(\xi, t))\sin n\theta]. \tag{2.38}$$

The infinite system given by (2.29), (2.30), (2.31), (2.32), (2.33), and (2.34) is made finite by truncating the stream and vorticity functions series in (2.37) and (2.38) at N. That is, we set

$$f_n(\xi) = F_n(\xi) = a_n(\xi, t) = A_n(\xi, t) = b_n(\xi, t) = B_n(\xi, t) = 0 \qquad \text{for} \quad n > N. \tag{2.39}$$

3. Numerical Solution Technique

The system of equations (2.29), (2.30), (2.31), (2.32), (2.33), and (2.34) was integrated numerically by the following steps:

(1) At time $t = 0$, we selected the disturbances which are modeled on the physically realizable system. In other words, $a_m(\xi, 0)$, $b_n(\xi, 0)$, $A_m(\xi, 0)$, and $B_n(\xi, 0)$ are known initially.

(2) The values of A_m and B_n on the surface of the cylinder can be explicitly obtained from (2.29) by using (2.35). These are given (Patel [13]) by

$$A_m(0, t) = \frac{2a_m(1, t)}{h^2} \qquad \text{for} \quad m = 0, 1, \ldots, N$$

and (3.1)

$$B_n(0, t) = \frac{2b_n(1, t)}{h^2} \qquad \text{for} \quad n = 1, 2, \ldots, N.$$

(3) Far away from the cylinder, the disturbed flow will not be necessarily symmetric and also we use a finite boundary, therefore, the smooth boundary conditions (Fornberg [7])

$$\frac{\partial \hat{\psi}}{\partial \xi}(\xi_\infty, t) = 0 \qquad \text{and} \qquad \frac{\partial \hat{\zeta}}{\partial \xi}(\xi_\infty, t) = 0$$

are used. This leads to

$$\frac{\partial a_m}{\partial \xi}(\xi_\infty, t) = \frac{\partial A_m}{\partial \xi}(\xi_\infty, t) = 0 \qquad \text{for} \quad m = 0, 1, \ldots, N$$

and (3.2)

$$\frac{\partial b_n}{\partial \xi}(\xi_\infty, t) = \frac{\partial B_n}{\partial \xi}(\xi_\infty, t) = 0 \qquad \text{for} \quad n = 1, 2, \ldots, N.$$

$(\partial a_m/\partial \xi)(\xi_\infty, t)$ is replaced by $(-3a_m(\xi_\infty, t) + 4a_m(\xi_{\infty-1}, t) - a_m(\xi_{\infty-2}, t))/2h$ in (3.2) and this gives

$$a_m(\xi_\infty, t) = \frac{(4a_m(\xi_{\infty-1}, t) - a_m(\xi_{\infty-2}, t))}{3} \qquad \text{for} \quad m = 0, 1, \ldots, N. \tag{3.3}$$

Similarly, one can get

$$A_m(\xi_\infty, t) = \frac{(4A_m(\xi_{\infty-1}, t) - A_m(\xi_{\infty-2}, t))}{3} \quad \text{for} \quad m = 0, 1, \ldots, N. \tag{3.4}$$

$(\partial\bar{\Psi}/\partial\xi)(\xi_\infty, t) = 0$ and $(\partial\bar{\zeta}/\partial\xi)\ (\xi_\infty, t) = 0$ are also used to generate the steady solutions.

Equations (2.30), (2.31), (2.32), (2.33), and (2.34) are solved by using the Crank–Nicolson method. By taking the average over the interval from t to $t + \Delta t$. (2.32) can be written as

$$\begin{aligned}
A_n^{t+\Delta t} = A_n^t + \Delta t \Bigg\{ & \frac{e^{-2\xi}}{\mathrm{Re}} \left[\left(\frac{\partial^2 A_n}{\partial \xi^2} - n^2 A_n \right)^{t+\Delta t} + \left(\frac{\partial^2 A_n}{\partial \xi^2} - n^2 A_n \right)^t \right] \\
& + \frac{e^{-2\xi}}{4} \left[(e^{\xi} - e^{-\xi}) \left\{ \left(\frac{\partial A_{n-1}}{\partial \xi} + \frac{\partial A_{n+1}}{\partial \xi} \right)^{t+\Delta t} + \left(\frac{\partial A_{n-1}}{\partial \xi} + \frac{\partial A_{n+1}}{\partial \xi} \right)^t \right\} \right. \\
& + (e^{\xi} + e^{-\xi}) \{ ((n+1) A_{n+1} - (n-1) A_{n-1})^{t+\Delta t} \\
& + ((n+1) A_{n+1} - (n-1) A_{n-1})^t \} \\
& + \sum_{m=1}^{N} m \left\{ \left[a_m \left(\frac{dF_{m+n}}{d\xi} + \frac{dF_{m-n}}{d\xi} + \frac{\partial B_{m+n}}{\partial \xi} + \frac{\partial B_{m-n}}{\partial \xi} \right) \right. \right. \\
& - A_m \left(\frac{df_{m+n}}{d\xi} + \frac{df_{m-n}}{d\xi} + \frac{\partial b_{m+n}}{\partial \xi} + \frac{\partial b_{m-n}}{\partial \xi} \right) \\
& - b_m \left(\frac{\partial A_{m+n}}{\partial \xi} + \frac{\partial A_{m-n}}{\partial \xi} \right) + B_m \left(\frac{\partial a_{m+n}}{\partial \xi} + \frac{\partial a_{m-n}}{\partial \xi} \right) \\
& \left. - f_m \left(\frac{\partial A_{m+n}}{\partial \xi} + \frac{\partial A_{m-n}}{\partial \xi} \right) + F_m \left(\frac{\partial a_{m+n}}{\partial \xi} + \frac{\partial a_{m-n}}{\partial \xi} \right) \right]^{t+\Delta t} \\
& + \left[a_m \left(\frac{dF_{m+n}}{d\xi} + \frac{dF_{m-n}}{d\xi} + \frac{\partial B_{m+n}}{\partial \xi} + \frac{\partial B_{m-n}}{\partial \xi} \right) \right. \\
& - A_m \left(\frac{df_{m+n}}{d\xi} + \frac{df_{m-n}}{d\xi} + \frac{\partial b_{m+n}}{\partial \xi} + \frac{\partial b_{m-n}}{\partial \xi} \right) - b_m \left(\frac{\partial A_{m+n}}{\partial \xi} + \frac{\partial A_{m-n}}{\partial \xi} \right) \\
& + B_m \left(\frac{\partial a_{m+n}}{\partial \xi} + \frac{\partial a_{m-n}}{\partial \xi} \right) - f_m \left(\frac{\partial A_{m+n}}{\partial \xi} + \frac{\partial A_{m-n}}{\partial \xi} \right) \\
& \left. \left. \left. + F_m \left(\frac{\partial a_{m+n}}{\partial \xi} + \frac{\partial a_{m-n}}{\partial \xi} \right) \right]^t \right\} \right] \Bigg\} \qquad \text{for} \quad n = 2, 3, \ldots, N.
\end{aligned} \tag{3.5}$$

By replacing the space derivatives by the central differences in (3.5), one gets the tridiagonal system for A_n and this tridiagonal system along with (3.1) and (3.4) is solved by the direct factorization method (Na [10]).

(4) The system (2.29) along with the boundary conditions

$$a_m(0, t) = \frac{\partial a_m}{\partial \xi}(\xi_\infty, t) = 0 \qquad \text{for} \quad m = 0, 1, \ldots, N$$

and

$$b_n(0, t) = \frac{\partial b_n}{\partial \xi}(\xi_\infty, t) = 0 \qquad \text{for} \quad n = 1, 2, \ldots, N \tag{3.6}$$

form the system of two-point boundary value problems for a_m and b_n. The left-hand sides of (2.29) contains A_m and B_n whose values at all points in the field of computation are known at each time step. This is solved by the Hermitian method as described by Collatz [1]. Let h be the spatial step of discretization and y_i, y_i' and y_i'' be the values of y, its first and second derivatives at node i. Then

$$y_{i-1}'' + 10y_i'' + y_{i+1}'' = \frac{12}{h^2}(y_{i-1} - 2y_i + y_{i+1}) + O(h^4). \tag{3.7}$$

The equation

$$\frac{\partial^2 a_m}{\partial \xi^2} - m^2 a_m = e^{2\xi} A_m \qquad \text{for} \quad m = 0, 1, \ldots, N$$

can be written by using (3.7) as

$$\left(1 - \frac{m^2h^2}{12}\right) a_m(\xi_{i-1}, t) - 2\left(1 + \frac{5m^2h^2}{12}\right) a_m(\xi_i, t) + \left(1 - \frac{m^2h^2}{12}\right) a_m(\xi_{i+1}, t)$$
$$= \frac{h^2}{12}\left[e^{2\xi_{i-1}} A_m(\xi_{i-1}, t) + 10e^{2\xi_i} A_m(\xi_i, t) + e^{2\xi_{i+1}} A_m(\xi_{i+1}, t)\right]$$
$$\text{for} \quad m = 0, 1, \ldots, N. \tag{3.8}$$

Equation (3.8) with boundary conditions (3.3) and (3.6) reduces to the tridiagonal system which is solved by the direct factorization method. Thus a_m is computed at all points in the field of computation and similarly b_n is also computed.

(5) Time was increased by Δt; i.e., $t_{\text{new}} = t_{\text{old}} + \Delta t$.

(6) Step (2) was repeated.

All of these steps were repeated at further times.

4. Results, Discussion, and Conclusion

The computations were carried out for values of the parameters shown in Table I on the Cyber 170/720 system at Humboldt State University, Arcata. The steady

TABLE I

Re	N	$h=\Delta\xi$	r_∞	α	t
10	20	$\pi/40$	102.909	4.00	0.01
20	20	$\pi/40$	102.909	4.00	0.01
40	40	$\pi/40$	102.909	0.25	0.01
100	25	$\pi/40$	102.909	0.25	0.01

solutions are obtained as a limit of the solutions of the time-dependent equations by the finite series truncation method as basically described by Patel [12].

In order to study the stability, we have to disturb the steady flow. The disturbance must satisfy the boundary conditions (2.20) and (2.21) and must be compatible with the present scheme. We have the steady flow around the cylinder and in order to disturb the flow, let us give an impulsive velocity $V_x=0$ and $V_y=\alpha$ to the surface of the cylinder where V_x and V_y are the velocity components in the x and y directions and α is a constant. This displaces the steady flow and the disturbance starts at $t=0$. V_x and V_y are given in terms of u and v by

$$V_x = u\cos\theta - v\sin\theta \qquad \text{and} \qquad V_y = u\sin\theta + v\cos\theta. \tag{4.1}$$

Using (2.4), (2.7), (2.12), (2.22), and (2.27) along with $r=e^{\xi}$ in (4.1), one gets the impulsive velocity components

$$\begin{aligned} V_x(\xi,\theta,t^*)\,|_{\xi=0} = &-1+\cos 2\theta+\cos\theta\sum_{n=1}^{N} n \\ &\times\left[-a_n(0,t^*)\sin n\theta+(b_n(0,t^*)+f_n(0,t^*))\cos n\theta\right] \\ &+\sin\theta\left\{\frac{\partial a_0}{\partial\xi}(0,t^*)+\sum_{n=1}^{N}\left[\frac{\partial a_n}{\partial\xi}(0,t^*)\cos n\theta\right.\right. \\ &\left.\left.+\left(\frac{\partial b_n}{\partial\xi}(0,t^*)+\frac{\partial f_n}{\partial\xi}(0,t^*)\right)\sin n\theta\right]\right\} \end{aligned} \tag{4.2}$$

and

$$\begin{aligned} V_y(\xi,\theta,t^*)\,|_{\xi=0} = &\sin 2\theta+\sin\theta\sum_{n=1}^{N} n \\ &\times\left[-a_n(0,t^*)\sin n\theta+(b_n(0,t^*)+f_n(0,t^*))\cos n\theta\right] \\ &-\cos\theta\left\{\frac{\partial a_0}{\partial\xi}(0,t^*)+\sum_{n=1}^{N}\left[\frac{\partial a_n}{\partial\xi}(0,t^*)\cos n\theta\right.\right. \\ &\left.\left.+\left(\frac{\partial b_n}{\partial\xi}(0,t^*)+\frac{\partial f_n}{\partial\xi}(0,t^*)\right)\sin n\theta\right]\right\} \end{aligned}$$

of the surface of the cylinder as $t^* \to 0$. Thus $V_x(\xi, \theta, t^*)|_{\xi=0} = 0$ and $V_y(\xi, \theta, t^*)|_{\xi=0} = \alpha$ gives only two equations to determine $a_0(0, t^*)$, $b_n(0, t^*)$, $a_n(0, t^*)$, $(\partial a_0/\partial\xi)(0, t^*)$, $(\partial b_n/\partial\xi)(0, t^*)$, and $(\partial a_n/\partial\xi)(0, t^*)$ and, therefore we arbitrarily select $a_0(0, t^*) = (\partial a_0/\partial\xi)(0, t^*) = 0$, $b_n(0, t^*) = (\partial b_n/\partial\xi)(0, t^*) = 0$ for $n = 1, 2, \ldots, N$ and $a_m(0, t^*) = (\partial a_m/\partial\xi)(0, t^*) = 0$ for $m = 2, 3, \ldots, N$ and substitute in (4.2). This leads to

$$\left(\frac{\partial a_1}{\partial \xi}(0, t^*) - a_1(0, t^*)\right) \sin\theta \cos\theta = 0$$

and (4.3)

$$a_1(0, t^*) \sin^2\theta + \frac{\partial a_1}{\partial \xi}(0, t^*) \cos^2\theta = \alpha.$$

This gives $(\partial a_1/\partial\xi)(0, t^*) = a_1(0, t^*) = \alpha$ and using a forward difference in $(\partial a_1/\partial\xi)(0, t^*) = \alpha$, one gets

$$a_1(h, t^*) = \alpha(1 + h). \tag{4.4}$$

Initially we selected

$$a_1(h, 0) = \alpha(1 + h) \tag{4.5}$$

and the rest of a_n and b_n equal to zero. Using (4.5) in (3.1) gives

$$A_1(0, 0) = \frac{2\alpha(1 + h)}{h^2} \tag{4.6}$$

and the rest of A_n and B_n equal to zero.

Thus (4.6) are the initial conditions for the parabolic partial differential equations (2.30), (2.31), (2.32), (2.33), and (2.34). Equations (4.5) and (4.6) correspond to the impulsive velocity $V_y = \alpha$ of the surface of the cylinder. The values of α and time step Δt used for calculations for various Reynolds numbers are also given in Table I. The values of the drag coefficient C_D and the lift coefficient C_L are computed (Patel [13]) from

$$C_D = \frac{4\pi}{\mathrm{Re}}\left(\frac{\partial F_1}{\partial \xi} + \frac{\partial B_1}{\partial \xi} - F_1 - B_1\right)\Bigg|_{\xi=0}$$

and (4.7)

$$C_L = \frac{4\pi}{\mathrm{Re}}\left(-2\frac{\partial A_0}{\partial \xi} + \frac{\partial A_1}{\partial \xi} - A_1\right)\Bigg|_{\xi=0}.$$

The boundary conditions

$$\frac{\partial \Psi}{\partial \xi} = 0 \quad \text{and} \quad \frac{\partial \zeta}{\partial \xi} = 0 \quad \text{as } \xi \to \infty \text{ are imposed at } r_\infty = 102.909.$$

TABLE II

Re	N	r_∞	C_D	L	ϕ
20	20	111.318	2.018	2.865	136.22°
20	20	102.909	2.016	2.865	136.22°
20	20	87.950	2.013	2.864	136.23°
40	40	102.909	1.504	5.433	126.37°
40	40	87.950	1.502	5.433	126.37°

In order to check whether this distance is far enough, we moved r_∞ in and out and checked whether the flow picture changes significantly. The results of some parameters for the steady solutions are given in Table II where L is the distance from the center of the cylinder to the tip of the eddy and ϕ is the angular distance of the point at which the streamline leaves the surface of the cylinder from the front stagnation point. The values of the coordinates of two points on the streamline $\Psi = 0.0$ with the same height from the axis of symmetry at various times are given in Table III for $\mathrm{Re} = 20$ and $\alpha = 4.0$ when the boundary conditions were imposed at different r_∞. The values of V_x, V_y, and $V = \sqrt{V_x^2 + V_y^2}$ at two symmetrically opposite points about the axis of symmetry with the given x and y coordinates in the wake at various times for $\mathrm{Re} = 40$ and $\alpha = 0.25$ are given in Table IV for different r_∞.

For $\mathrm{Re} = 40$ and $\alpha = 0.25$, r_∞ was not moved out because of the limited size of the computer memory. There is not a significant change in the flow field as we move r_∞ in and out as can be seen from Tables II–IV and, therefore, the choice of $r_\infty = 102.909$ is probably safe. All calculations presented are carried out by using $r_\infty = 102.909$.

Some of the results for the steady solutions along with the results of others are given in Table V for comparison. The values of C_D and L for $\mathrm{Re} = 20$ and 40 are in

TABLE III

t	r_∞	x	y
30	111.318	−2.814	0.049
		−2.813	−0.049
	102.909	−2.813	0.049
		−2.812	−0.049
	87.950	−2.813	0.049
		−2.811	−0.049
40	111.318	−2.833	0.049
		−2.796	−0.049
	102.909	−2.832	0.049
		−2.796	−0.049
	87.950	−2.832	0.049
		−2.795	−0.049

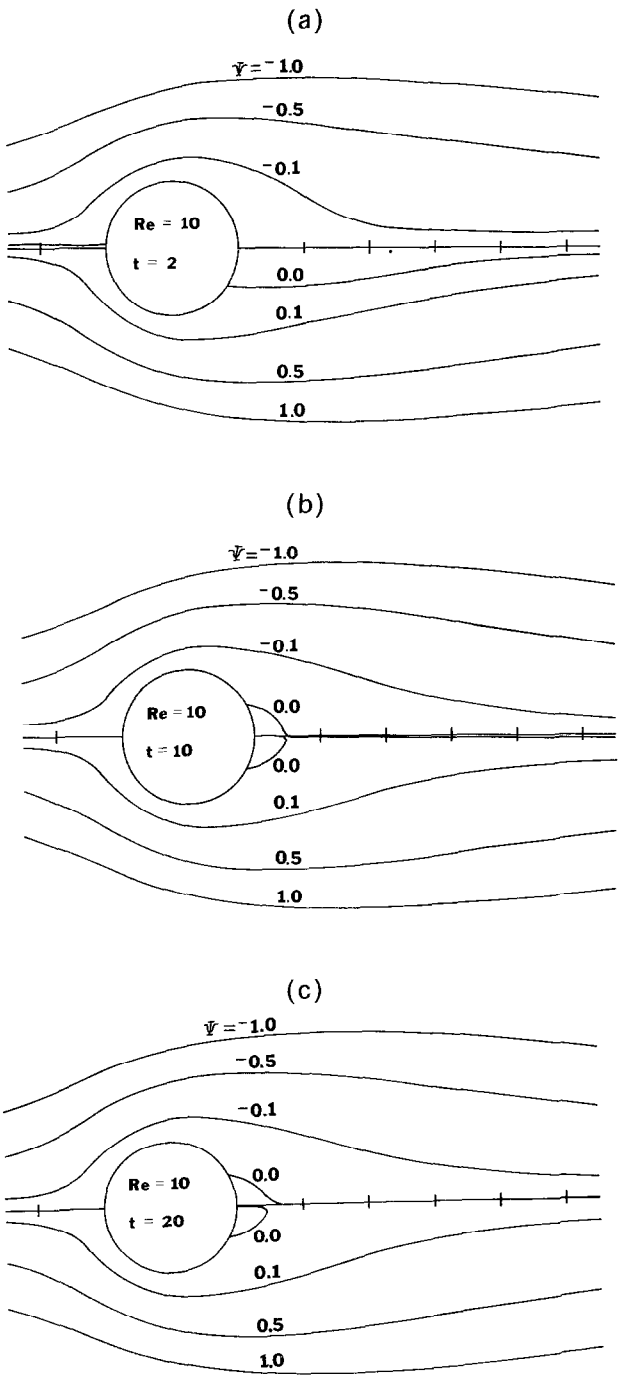

FIG. 1. The development of the streamlines with time for Re = 10 and $\alpha = 4.0$.

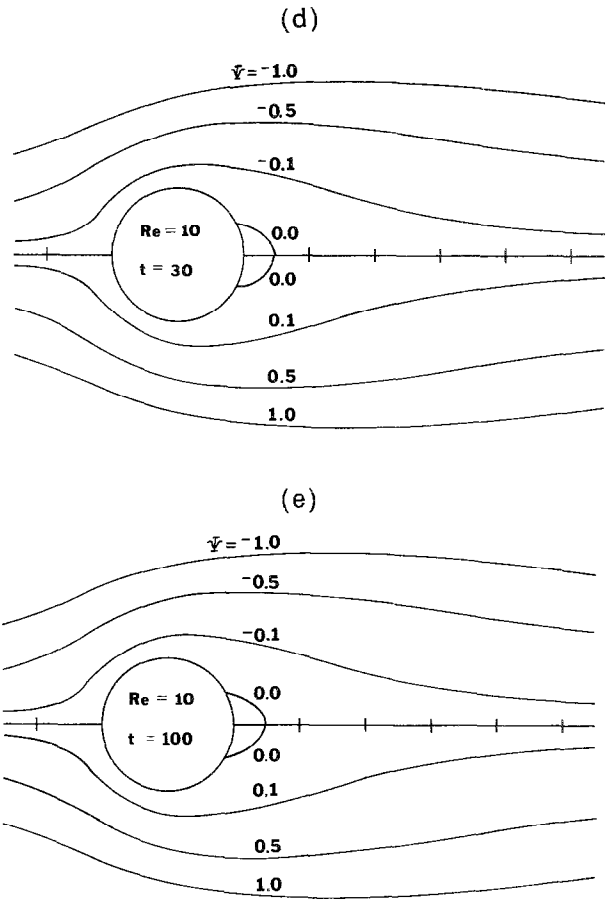

FIGURE 1—*Continued*

TABLE IV

t	r_∞	x	y	$10V_r$	$10V_\theta$	$10V$
2	102.909	−5.203	0.091	0.469	−0.015	0.469
		−5.203	−0.091	0.400	−0.346	0.529
	87.950	−5.203	0.091	0.469	−0.002	0.469
		−5.203	−0.091	0.400	−0.340	0.525
10	102.909	−5.203	0.091	1.516	0.112	1.520
		−5.203	−0.091	1.537	−0.206	1.551
	87.950	−5.203	0.091	1.516	0.107	1.519
		−5.203	−0.091	1.537	−0.201	1.550
20	102.909	−5.203	0.091	0.053	0.181	0.188
		−5.203	−0.091	0.043	−0.174	0.179
	87.950	−5.203	0.091	0.053	0.175	0.183
		−5.203	−0.091	0.043	−0.169	0.174

TABLE V

Reference	Re	C_D	L	ϕ
Taneda [17]	10	—	1.6	—
	20	—	2.8	—
	40	—	5.2	127°
Underwood [20]	10	3.5	1.24	150°
Dennis and	10	2.846	1.53	150.40°
Chang [4]	20	2.045	2.88	136.30°
	40	1.522	5.69	126.20°
Nieuwstadt and	10	2.8283	1.434	152.04°
Keller [11]	20	2.0530	2.786	136.63°
	40	1.5504	5.357	126.66°
Coutanceau and	10	—	1.68	147.50°
Bouard [3]	20	—	2.86	135.20°
	40	—	5.26	126.50°
Fornberg [7]	20	2.0001	2.82	134.86°
	40	1.4980	5.48	124.79°
Jafroudi and	10	2.647	—	159.722°
Yang [9]	20	1.927	—	138.667°
	40	1.555	—	128.578°
Present paper	10	2.839	1.513	150.60°
	20	2.014	2.864	136.22°
	40	1.504	5.433	126.37°

good agreement with those of Fornberg [7] while the values of C_D, L, and ϕ for Re = 10, 20, and 40 reasonably agree with those of Dennis and Chang [4].

Reynolds Number 10

The development of the streamlines for the Reynolds number 10 with $N = 20$ and $\alpha = 4.0$ at various times is shown in Fig. 1. At $t = 2$, the streamline $\Psi = 0.0$ has moved upward on the side of the inflow and moved downward on the side of the outflow and the vortices are not seen. At $t = 10$ and 20, two vortices are clearly seen in Figs. 1b and c. Almost symmetrical wakes are seen at $t = 30$ in Fig. 1d. The

TABLE VI

t	x	y	t	x	y
30	−1.495	0.026	70	−1.487	0.026
	−1.477	−0.026		−1.486	−0.026
40	1.488	0.026	80	−1.487	0.026
	−1.485	−0.026		−1.486	−0.026
50	−1.488	0.026	90	−1.488	0.026
	−1.486	−0.026		−1.486	−0.026
60	−1.488	0.026	100	−1.488	0.026
	−1.486	−0.026		−1.486	−0.026

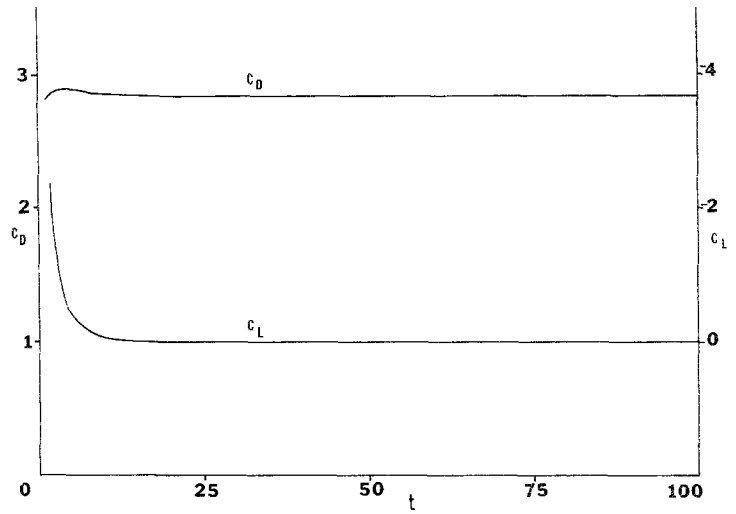

FIG. 2. The development of C_D and C_L with time for Re = 10 and $\alpha = 4.0$.

values of the coordinates of two points on the streamline $\Psi = 0.0$ with the same height from the axis of symmetry are given in Table VI at various times.

It can be seen from the values of the coordinates from Table VI that the upper vortex is almost equal to the lower vortex. Almost symmetrical streamlines are seen at $t = 100$ in Fig. 1e. It is clear that the disturbance has not died out completely for a long time, and it is doubtful that the flow will ever be symmetrical in the strictest sense. The development of the drag coefficient C_D and the lift coefficient C_L is given in Fig. 2.

Reynolds Number 20

[redacted] side of the outflow and moved upward on the side of the inflow. The vortices are completely gone. In Figs. 3b and c at $t = 10$ and 20 two vortices are seen but they

TABLE VII

t	x	y	t	x	y
30	−2.813	0.049	70	−2.820	0.049
	−2.812	−0.049		−2.810	−0.049
40	−2.832	0.049	80	−2.812	0.049
	−2.796	−0.049		−2.818	−0.049
50	−2.838	0.049	90	−2.809	0.049
	−2.791	−0.049		−2.822	−0.049
60	−2.830	0.049	100	−2.807	0.049
	−2.800	−0.049		−2.823	−0.049

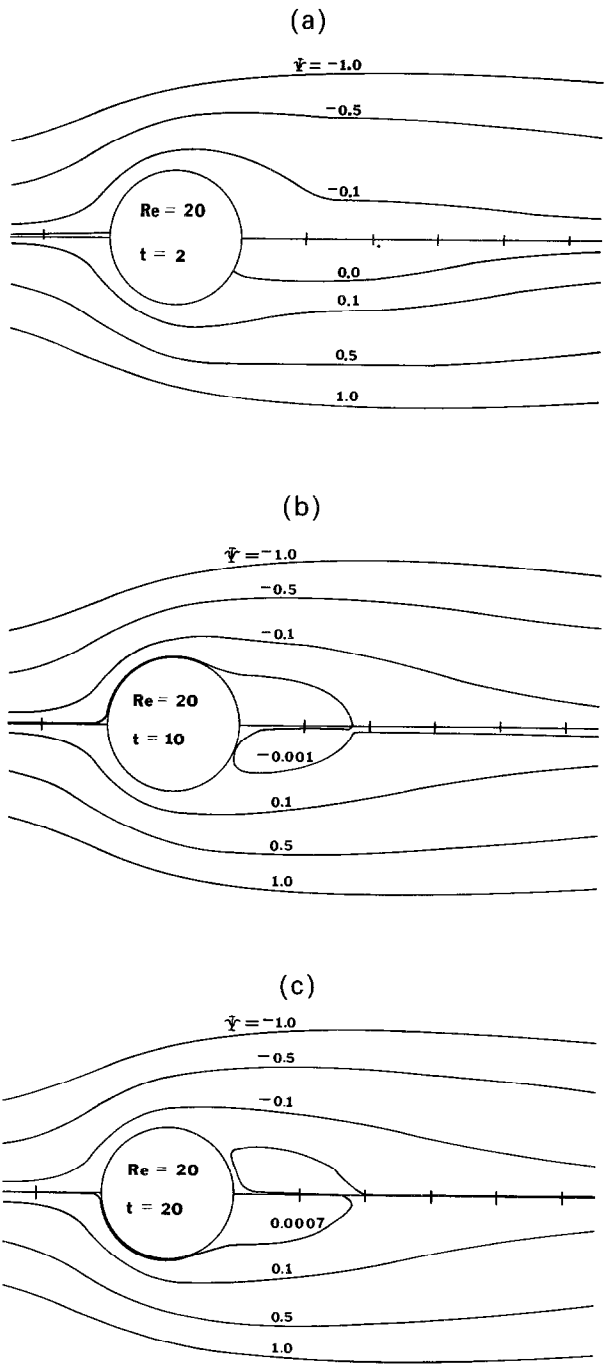

FIG. 3. The development of the streamlines with time for Re = 20 and $\alpha = 4.0$.

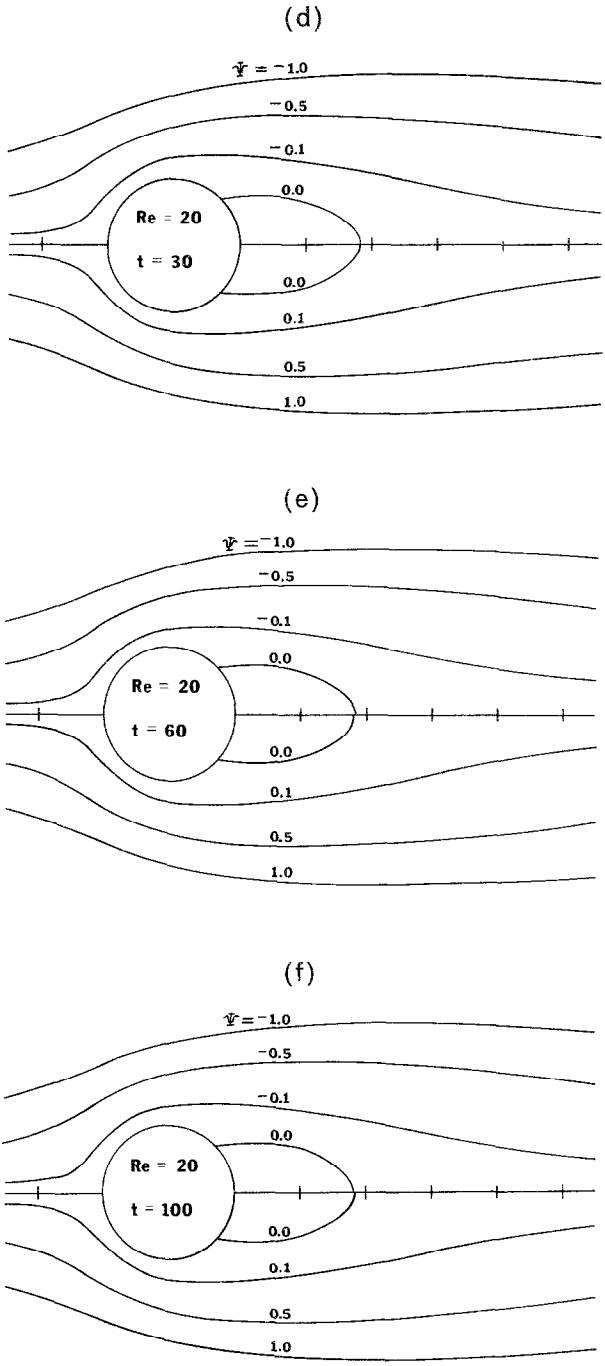

FIGURE 3—*Continued*

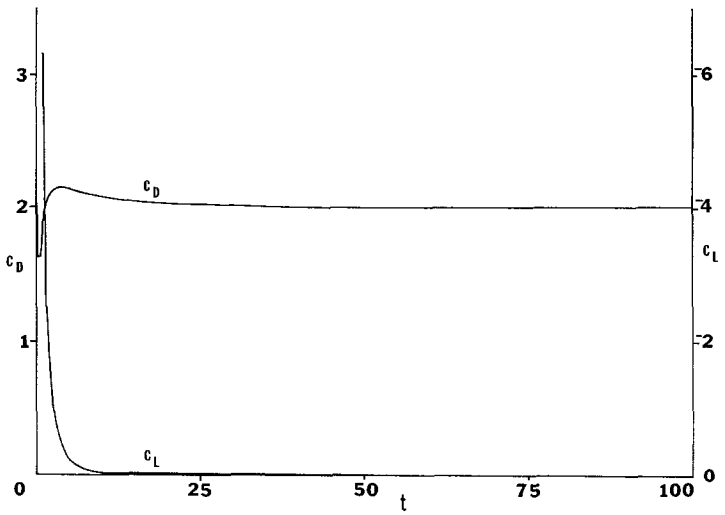

FIG. 4. The development of C_D and C_L with time for Re = 20 and $\alpha = 4.0$.

TABLE VIII

t	x	y	$10V_x$	$10V_y$	$10V$
2	−5.203	0.091	0.469	−0.015	0.469
	−5.203	−0.091	0.400	−0.346	0.529
10	−5.203	0.091	1.516	0.112	1.520
	−5.203	−0.091	1.537	−0.206	1.551
20	−5.203	0.091	0.053	0.181	0.188
	−5.203	−0.091	0.043	−0.174	0.179
30	−5.203	0.091	0.089	0.188	0.208
	−5.203	−0.091	0.088	−0.174	0.195
40	−5.203	0.091	0.075	0.185	0.200
	−5.203	−0.091	0.083	−0.182	0.200
50	−5.203	0.091	0.072	0.179	0.193
	−5.203	−0.091	0.069	−0.191	0.203
60	−5.203	0.091	0.068	0.178	0.191
	−5.203	−0.091	0.063	−0.194	0.204
70	−5.203	0.091	0.065	0.178	0.190
	−5.203	−0.091	0.060	−0.196	0.205
80	−5.203	0.091	0.064	0.179	0.190
	−5.203	−0.091	0.058	−0.196	0.204
91	−5.203	0.091	0.062	0.181	0.191
	−5.203	−0.091	0.057	−0.194	0.202
100	−5.203	0.091	0.061	0.183	0.193
	−5.203	−0.091	0.057	−0.192	0.201

oscillate alternately. Figure 3d shows approximately symmetrical streamlines at $t = 30$.

Table VII gives the values of the coordinates of two points with the same height from the axis of symmetry on the streamline $\Psi = 0.0$ at various times. The lengths of the vortices are not equal; though at $t = 30$ and 80, they are almost equal. From Table VII, it can be seen that at $t = 40$, 50, 60, and 70 the upper vortex is slightly longer than the lower vortex; also, this can be seen in Fig. 3e at $t = 60$. At $t = 80$, 90, and 100, the lower vortex is slightly longer than the upper one. This is represented in Fig. 3f at $t = 100$. It is clear that the wake trails oscillate slightly and the flow is not symmetrical in the strictest sense of symmetry. In Fig. 4, the development of the drag coefficient C_D and the lift coefficient C_L is given.

Reynolds Number 40

The development of the flow pattern for $\mathrm{Re} = 40$ with $N = 40$ and $\alpha = 0.25$ at various times is shown in Fig. 5. The numerical procedure breaks down for $\alpha > 0.5$. In Figs. 5a and b at $t = 2$ and 10, the vortices are shed; while, in Fig. 5c at $t = 20$, the disturbance begins to decay and the two standing eddies have begun to develop. At $t = 30$ and 40 in Figs. 5d and e, the wakes oscillate while at $t = 50$ and 60 in Figs. 5f and g, the disturbance seems to be dying and the flow seems to be restoring to the symmetrical form. Again, the oscillations of the wakes are seen at $t = 70$ and 80 in Figs. 5h and i. In Figs. 5j and k at $t = 91$ and 100 the wakes are not symmetrical. This can also be seen from Table VIII which gives the values of V_x, V_y, and $V = \sqrt{V_x^2 + V_y^2}$ at two symmetrically opposite points about the axis of symmetry with the given x and y coordinates in the wake at various times. It seems that the flow at $\mathrm{Re} = 40$ depends on the initial disturbance. The development of the drag coefficient C_D and the lift coefficient C_L is given in Fig. 6.

Reynolds Number 100

In order to check whether the initial disturbance triggers the vortex shedding, the computations were carried out for $\mathrm{Re} = 100$ with $N = 25$ and $\alpha = 0.25$ up to $t = 100$. The computations for higher N need more computer time and our interest is very limited, therefore, computations were not carried out for higher N. The results are shown in Fig. 7. At $t = 2$, only one vortex is seen in Fig. 7a. Figure 7b at $t = 10$ shows the development of two asymmetric vortices. One of the vortices is captured by the stream flow and this marks the beginning of the vortex shedding. In Figs. 7c and d at $t = 20$ and 30, vortex shedding is clearly seen; also vortices are shed alternately from the two sides of the cylinder. Vortex shedding continues as can be seen in Figs. 7e–k at $t = 40$, 50, 60, 70, 80, 90, and 100 alternately from the two sides of the cylinder. The initial disturbance is not decaying but, in fact, triggers the vortex shedding. In Fig. 8, the development of the lift coefficient C_L and the drag coefficient C_D is given.

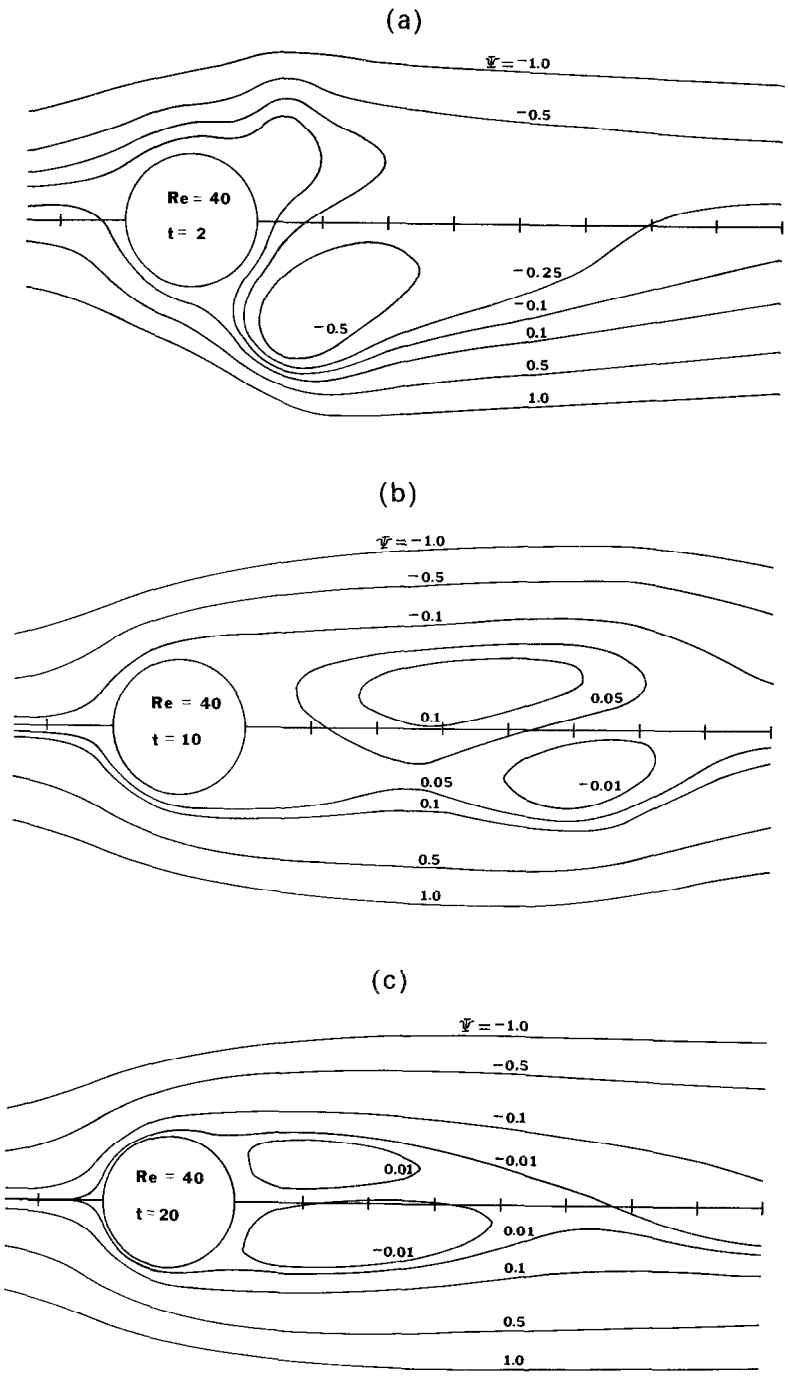

FIG. 5. The development of the streamlines with time for $\mathrm{Re} = 40$ and $\alpha = 0.25$.

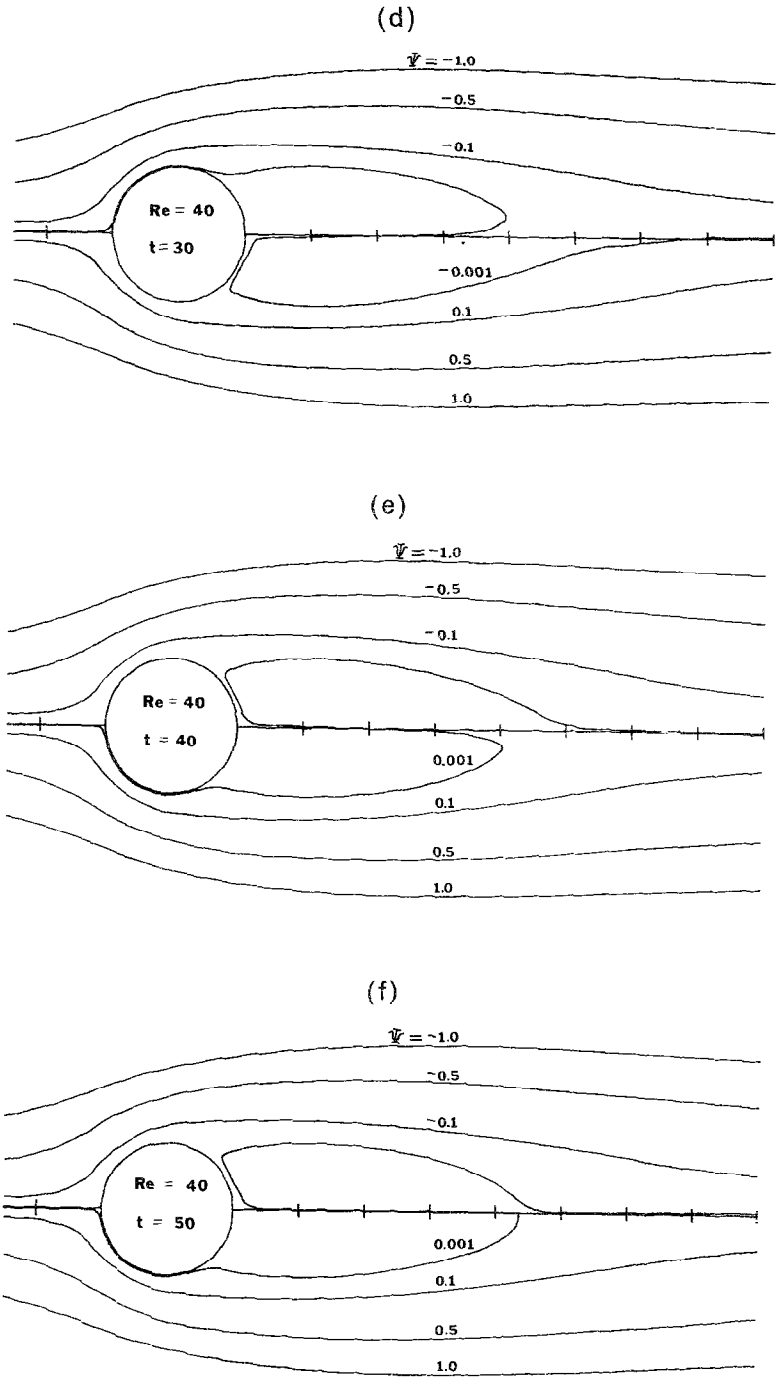

FIGURE 5—*Continued*

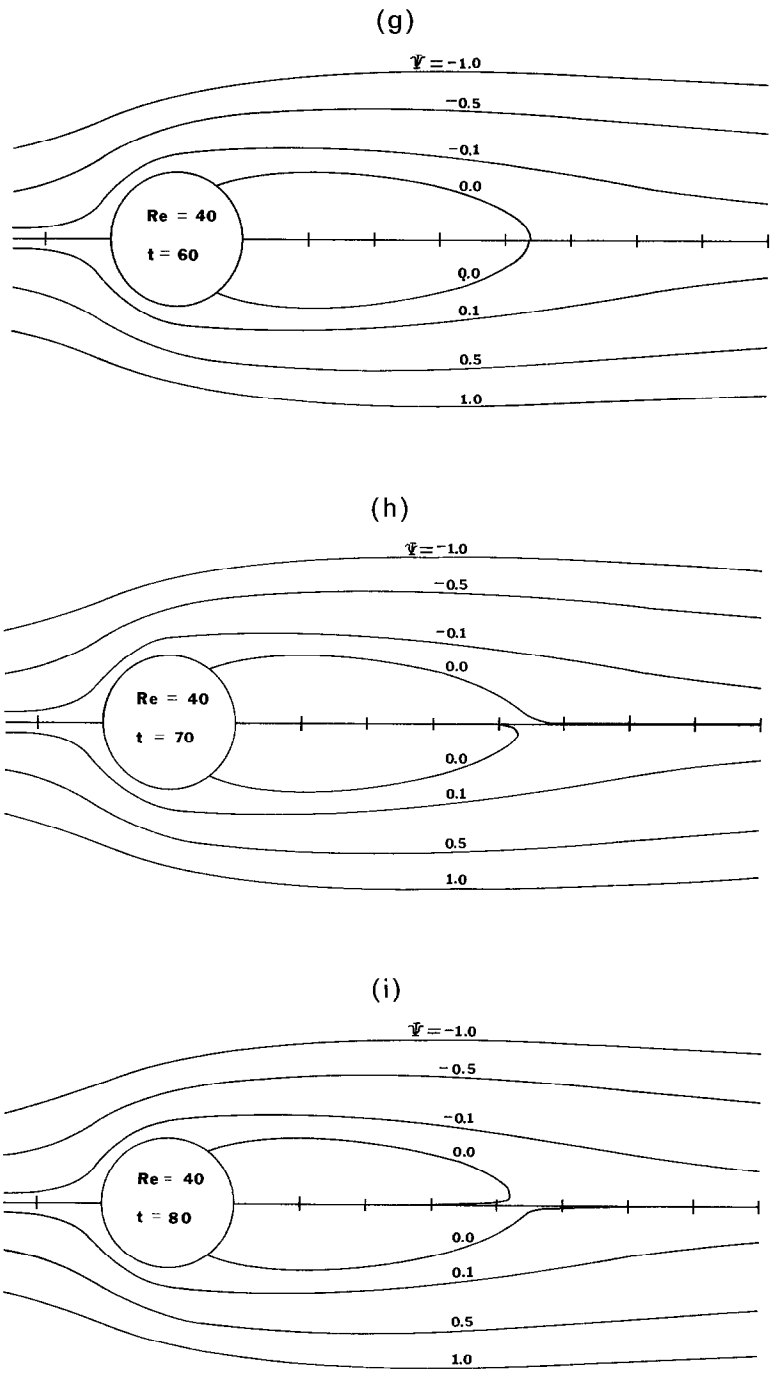

FIGURE 5—*Continued*

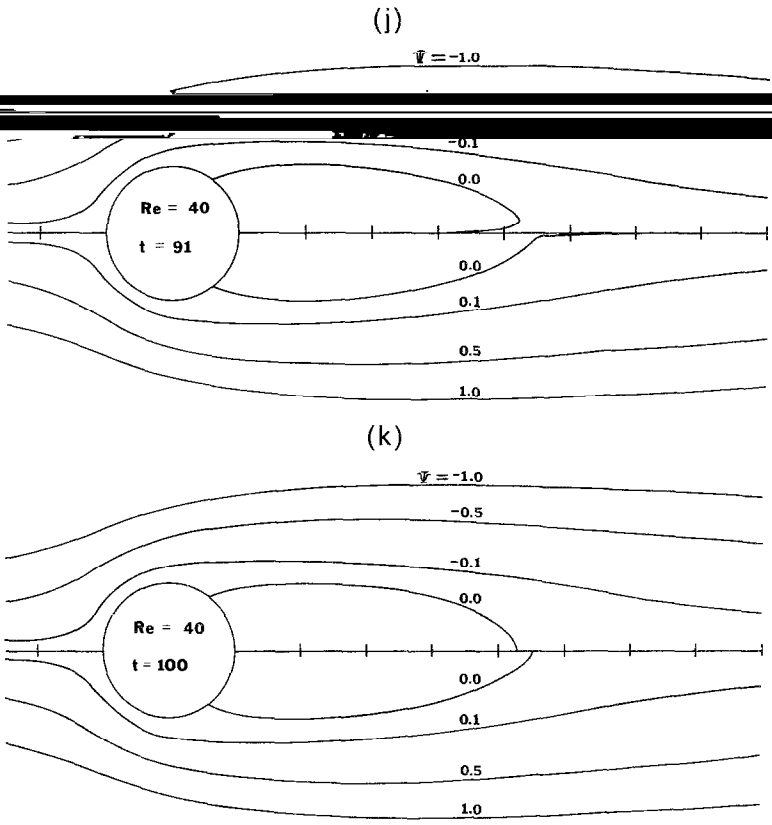

FIGURE 5—*Continued*

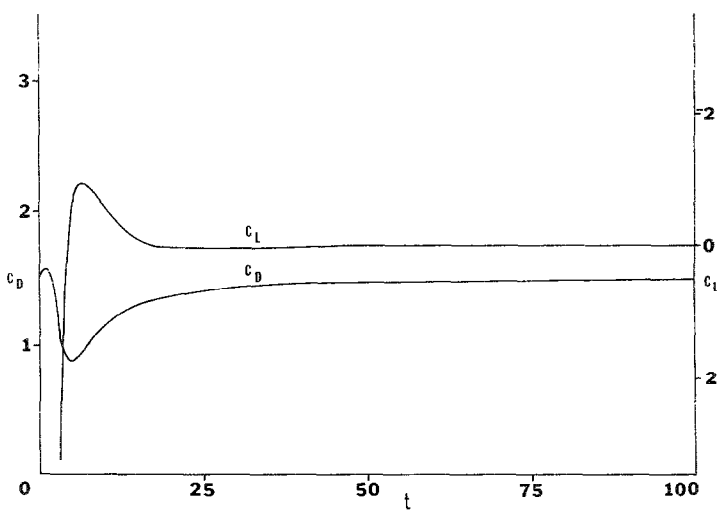

FIG.6. The development of C_D and C_L with time for $\mathrm{Re} = 40$ and $\alpha = 0.25$.

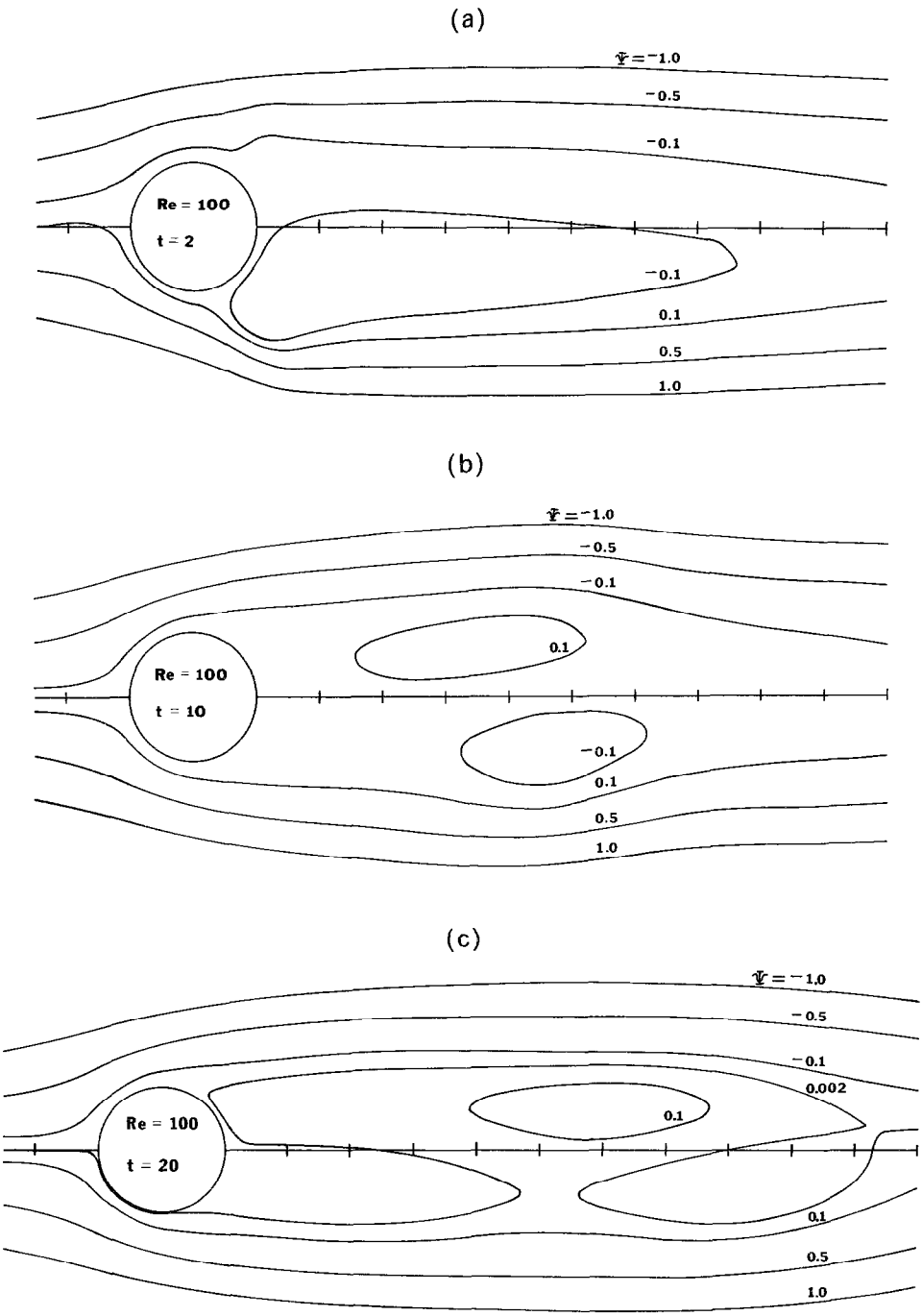

FIG. 7. The development of the streamlines with time for $\mathrm{Re} = 100$ and $\alpha = 0.25$.

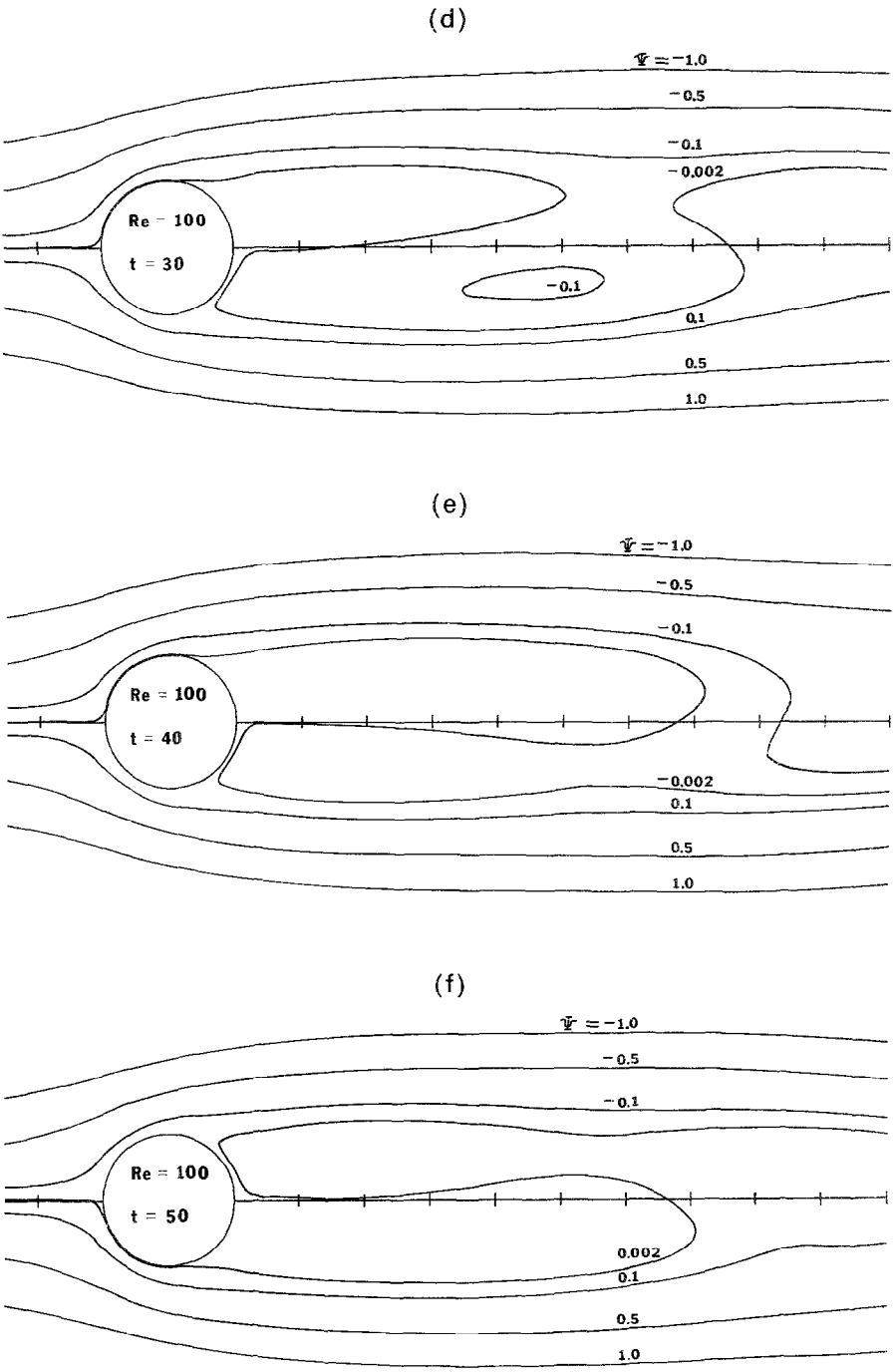

FIGURE 7—*Continued*

(g)

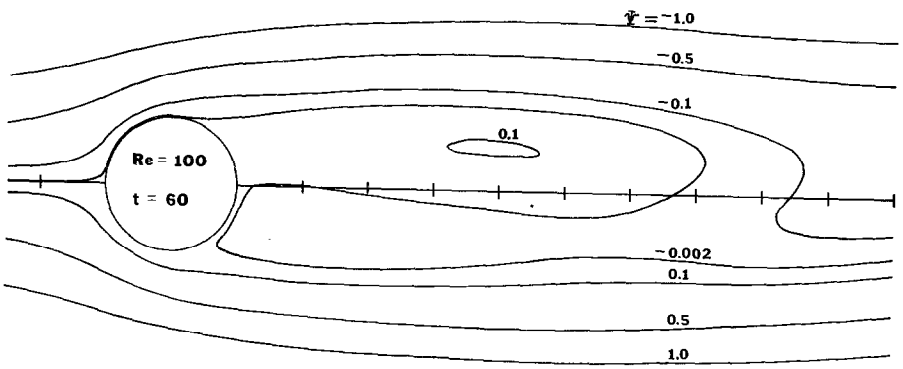

(h)

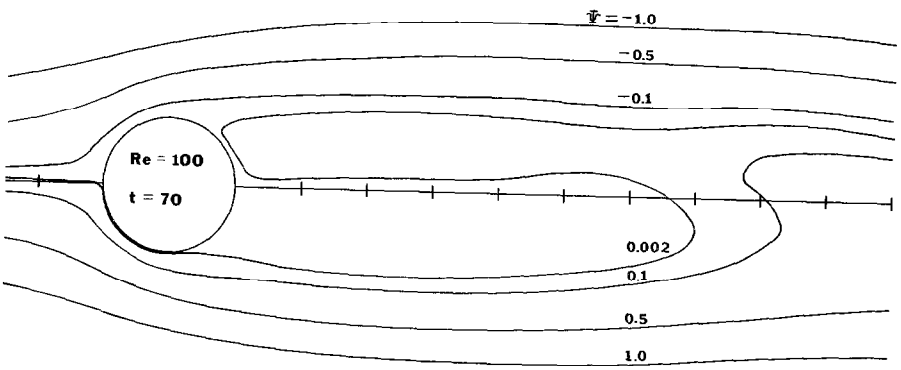

(i)

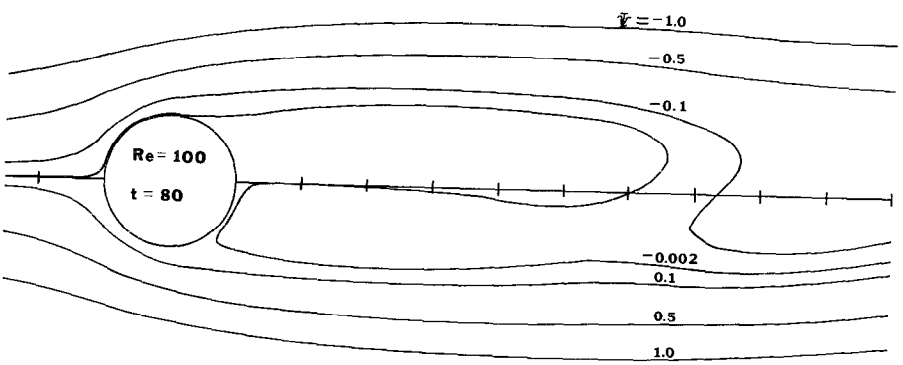

FIGURE 7—*Continued*

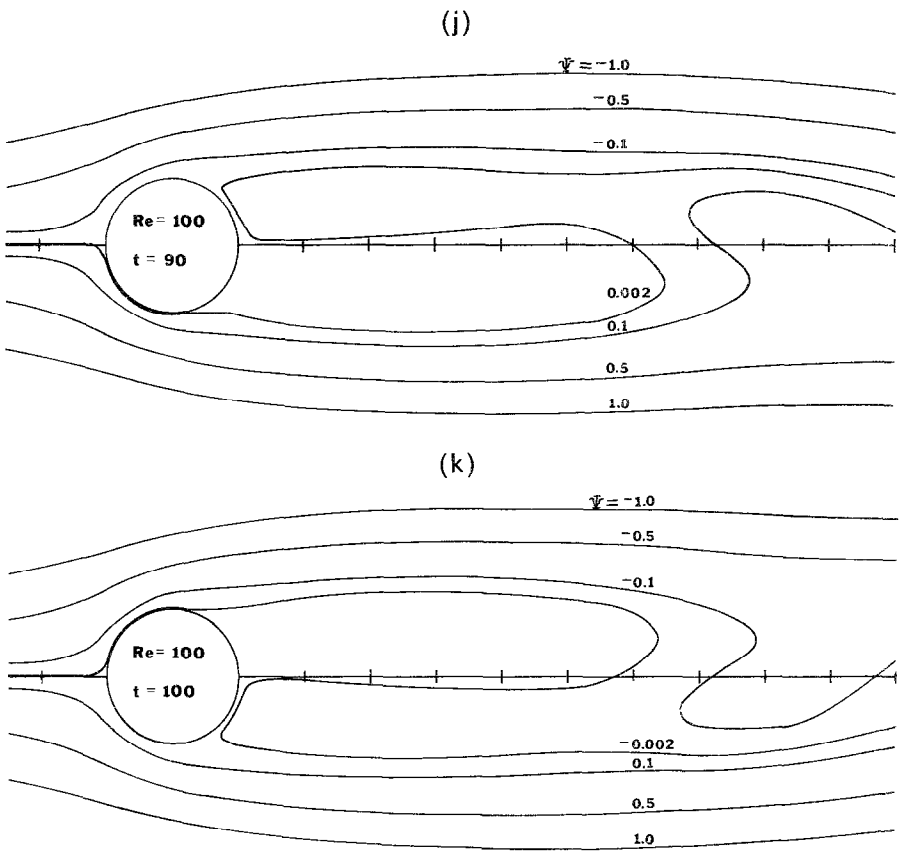

FIGURE 7—*Continued*

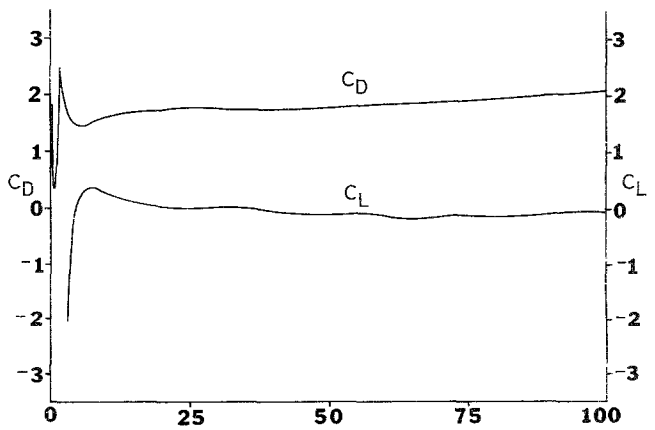

FIG. 8. The development of C_D and C_L with time for Re = 100 and $\alpha = 0.25$.

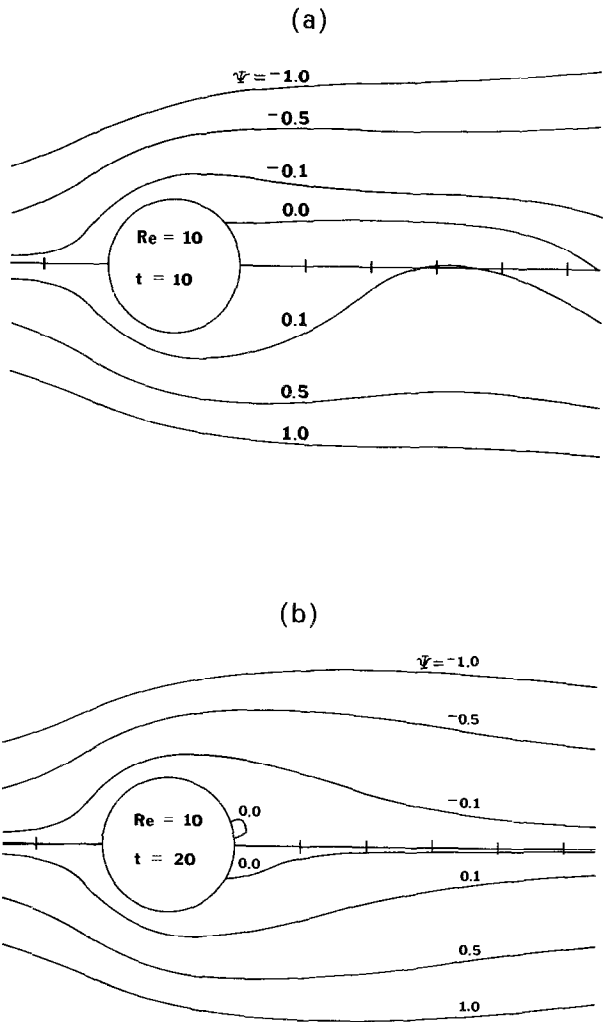

FIG. 9. The development of the streamlines with time for $Re = 10$ and $\alpha = 0.25$.

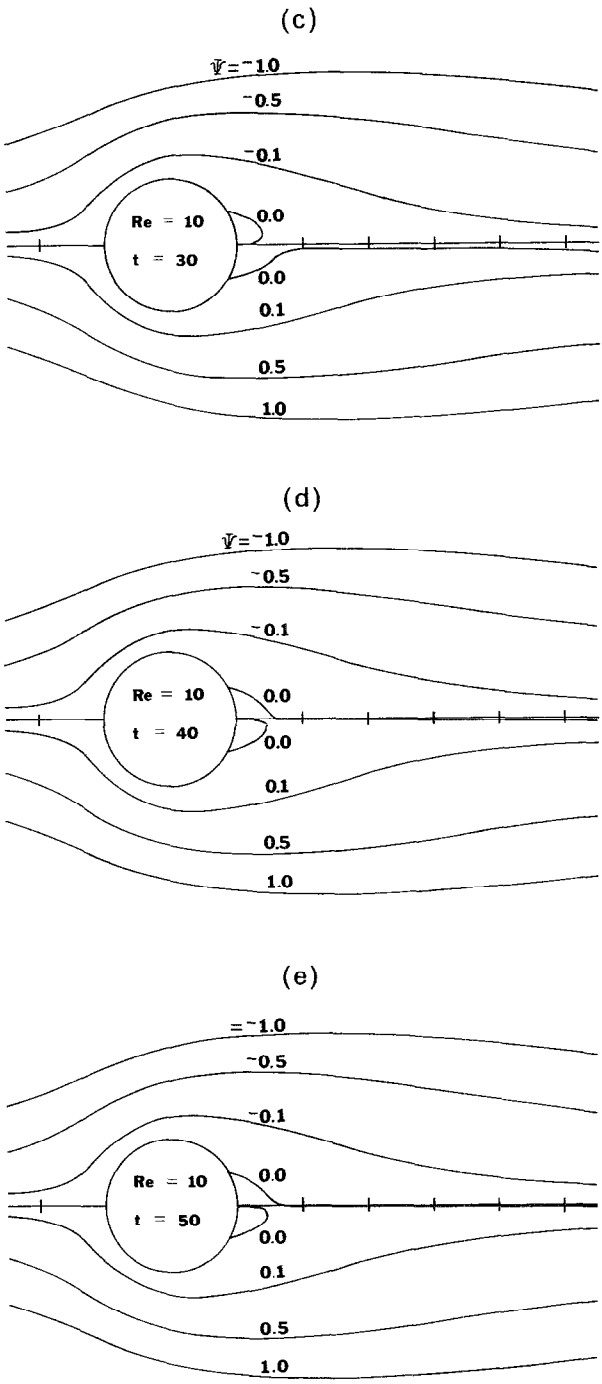

FIGURE 9—*Continued*

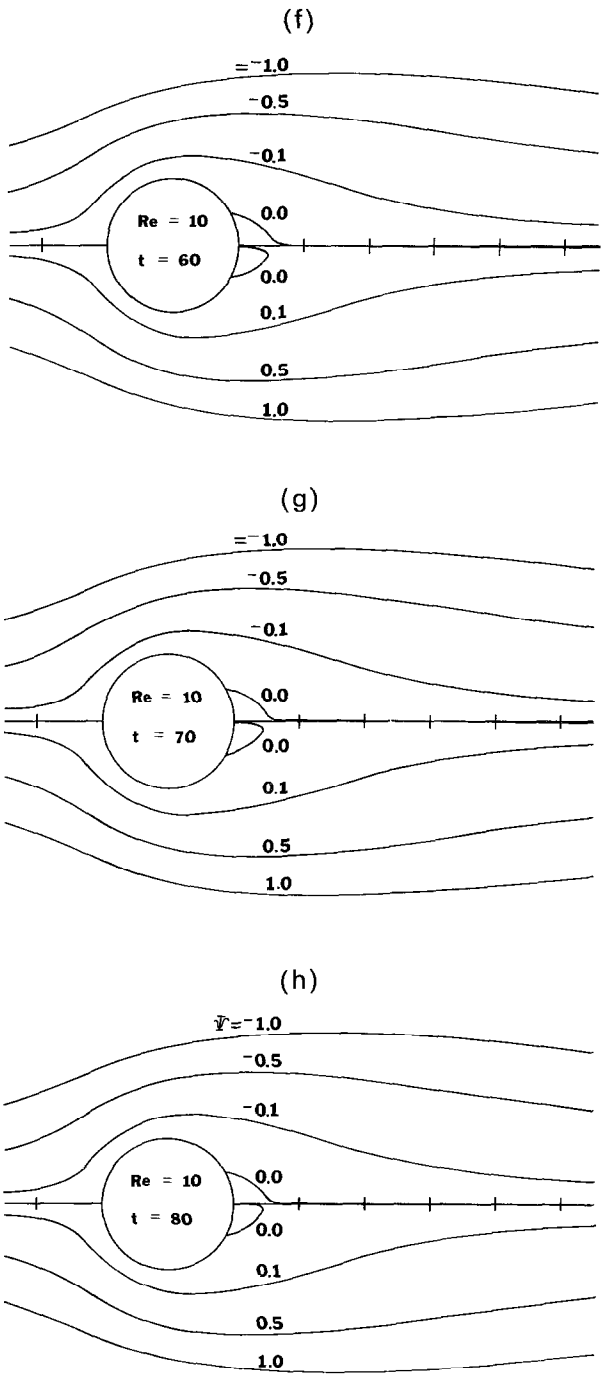

FIGURE 9—*Continued*

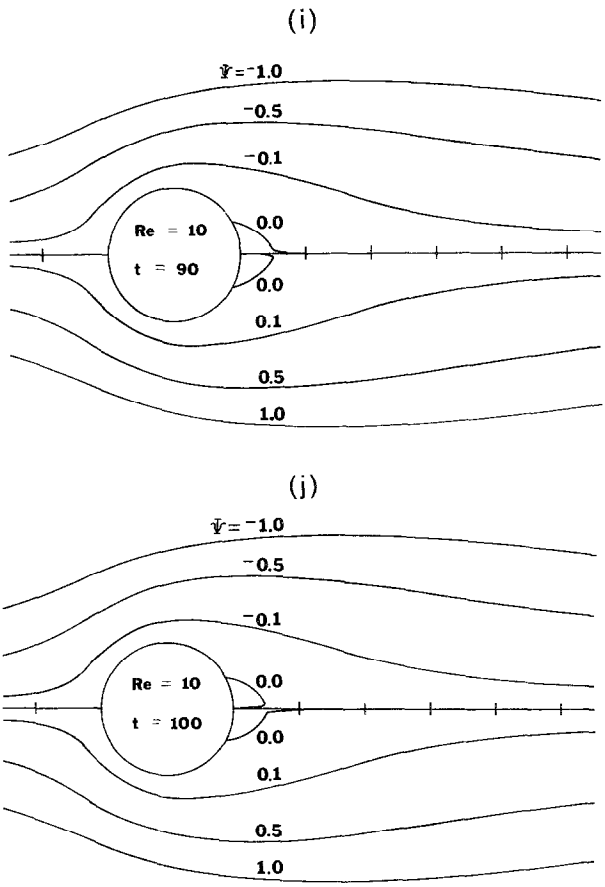

FIGURE 9—*Continued*

Reynolds Number 10

The initial disturbance (4.5) with $\alpha = 0.25$ was applied for $\mathrm{Re} = 10$ and $N = 20$ and then $a_1(h, t) = 0.25(1 + h)$ was used up to $t = 1$. This disturbance may correspond to an electromagnetic phenomena which gives impulsive velocity $V_x = 0$ and $V_y = \alpha$ to the cylinder up to $t = 1$ in the steady flow. The development of the streamlines are shown in Fig. 9 at various times. In Fig. 9a at $t = 10$, vortices are not seen. One developing vortex is seen in the upper part at $t = 20$ in Fig. 9b. At $t = 30$, one vortex in the upper part is seen in Fig. 9c, while Fig. 9d at $t = 40$ shows one vortex in the lower part of the flow. The vortex in the lower part remains until $t = 100$ as shown in Figs. 9e–i at $t = 50$, 60, 70, 80, and 90. At $t = 100$, the closed vortex is seen in the upper part of the flow in Fig. 9j and the flow has not restored to symmetrical form. The values of V_x, V_y, and $V = \sqrt{V_x^2 + \frac{2}{y}}$ are given in Table IX at two symmetrically opposite points about the axis of symmetry with the given x and y coordinates in the wake at various times and from those values, it is clear

TABLE IX

	−1.481	−0.026	0.049	2.721	2.721
10	−1.481	0.026	−0.036	−2.258	2.259
	−1.481	−0.026	−0.017	1.654	1.654
20	−1.481	0.026	−0.026	−1.934	1.934
	−1.481	−0.026	−0.027	1.833	1.833
30	−1.481	0.026	−0.028	−1.793	1.793
	−1.481	−0.026	−0.030	1.932	1.932
40	−1.481	0.026	−0.029	−1.784	1.784
	−1.481	−0.026	−0.031	1.925	1.925
50	−1.481	0.026	−0.030	−1.800	1.800
	−1.481	−0.026	−0.031	1.900	1.900
60	−1.481	0.026	−0.030	−1.817	1.817
	−1.481	−0.026	−0.031	1.880	1.880
70	−1.481	0.026	−0.030	−1.829	1.829
	−1.481	−0.026	−0.031	1.865	1.865
80	−1.481	0.026	−0.030	−1.838	1.838
	−1.481	−0.026	−0.031	1.855	1.855
90	−1.481	0.026	−0.030	−1.843	1.843
	−1.481	−0.026	−0.031	1.849	1.850
100	−1.481	0.026	−0.030	−1.846	1.846
	−1.481	−0.026	−0.031	1.847	1.847
110	−1.481	0.026	−0.030	−1.844	1.844
	−1.481	−0.026	−0.031	1.848	1.848
120	−1.481	0.026	−0.030	−1.840	1.841
	−1.481	−0.026	−0.031	1.852	1.852

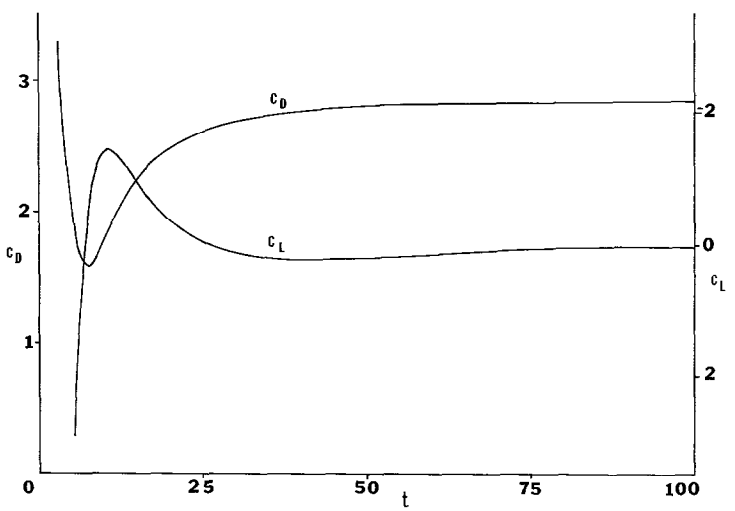

FIG. 10. The development of C_D and C_L with time for Re = 10 and $\alpha = 0.25$.

that even at $t = 120$ the flow is not symmetrical. In Fig. 10, the development of the drag coefficient C_D and the lift coefficient C_L is given. Since the disturbances have spread far away from the beginning, this keeps the flow asymmetric. The initial disturbance applied to the symmetric flow at Reynolds number 40 does not grow; however, initially, it triggers the vortex shedding. The flow remains unsteady and asymmetrical for a long time as observed experimentally. While the initial disturbance at $\mathrm{Re} = 100$ triggers the vortex shedding. In the case of Reynolds number 20, the trace of the initial disturbance oscillates the wake trails slightly. The flow does not become symmetric in the strictest sense even at Reynolds number 10 after a long time after the initial disturbance; on the other hand, by applying he disturbance continuously up to $t = 1$, we do not even have two nearly symmetrical wakes. It indicates that the symmetry of the flow around the cylinder depends upon the disturbance level in the flow. It is observed in this work that there exists an initial disturbance for which the flow at $\mathrm{Re} = 40$ is not symmetrical for a long time.

The computations were carried out for $\mathrm{Re} = 40$ and $\alpha = 0.25$ by using $N = 35$ and $N = 40$. The graphs of streamlines and equivorticity lines at $t = 2$, 10, and 20 were almost identical for $N = 35$ and 40. However, these values of N are not well separated.

REFERENCES

1. L. COLLATZ, *The Numerical Treatment of Differential Equations*, 3rd ed. (Springer-Verlag, New York, 1966), p. 164.
2. W. M. COLLINS AND S. C. R. DENNIS, *J. Fluid Mech.* **60**, 105 (1973).
3. M. COUTANCEAU AND R. BOUARD, *J. Fluid Mech.* **79**, 231 (1977).
4. S. C. R. DENNIS AND GAU-ZU CHANG, *J. Fluid Mech.* **42**, 471 (1970).
5. S. M. DESAI, Ph.D. thesis, University of California, Berkeley, 1965 (unpublished).
6. P. G. DRAZIN AND W. H. REID, *Hydrodynamic Stability* (Cambridge Univ. Press, Cambridge, 1981), p. 8.
7. B. FORNBERG, *J. Fluid Mech.* **98**, 819 (1980).
8. J. H. GERRARD, *Philos. Trans. Roy. Soc. A* **288**, 351 (1978).
9. H. JAFROUDI AND H. T. YANG, *J. Comput. Phys.* **49**, 181 (1983).
10. T. Y. NA, *Computational Methods in Engineering Boundary Value Problems* (Academic Press, New York, 1979), p. 98.
11. F. NIEUWSTADT AND H. B. KELLER, *Comput. Fluids* **1**, 59 (1973).
12. V. A. PATEL, *Comput. Fluids* **4**, 13 (1976).
13. V. A. PATEL, *J. Comput. Phys.* **28**, 14 (1978).
14. V. A. PATEL, *Comput. Fluids* **9**, 435 (1981).
15. A ROSKO, NACA Report No. 1191, 1954 (unpublished).
16. A. ROSKO, NACA Technical Note No. 3169, 1954 (unpublished).
17. S. TANEDA, *J. Phys. Soc. Japan* **11**, 302 (1956).
18. S. TANEDA, *J. Phys. Soc. Japan* **18**, 288 (1963).
19. D. J. TRITTON, *J. Fluid Mech.* **6**, 547 (1959).
20. R. L. UNDERWOOD, *J. Fluid Mech.* **37**, 95 (1969).